Vol 10 No 9, September 2001
1009-1963/2001/10(09)/0862-07

Chinese Physics

© 2001 Chin. Phys. Soc.
and IOP Publishing Ltd

ANISOTROPIC CHARACTERISTICS OF DEMAGNETIZATION CURVE FOR NANOCRYSTALLINE Nd–Fe–B MAGNET CALCULATED BY MICROMAGNETICS*

Jin Han-min(金汉民), Wang Xue-feng(王学凤),
Zhao Su-fen(赵素芬), and Yan Yu(闫 羽)
Department of Physics, Jilin University, Changchun 130023, *China*

(Received 16 December 2000; revised manuscript received 13 February 2001)

The demagnetization curves for nanocrystalline Nd–Fe–B magnets of a stoichiometric composition were calculated by making use of the finite element technique of micromagnetics. The curve, especially ${}_{\rm i}H_{\rm c}$, varies in a wide range with the direction of applied field if the grain number N is taken to be small. With the increase of N, the range becomes smaller and the average of ${}_{\rm i}H_{\rm c}$ decreases and approaches a limit ${}_{\rm i}H_{\rm c}(N=\infty)$. ${}_{\rm i}H_{\rm c}$ for finite N is larger than, or at least equal to, ${}_{\rm i}H_{\rm c}(N=\infty)$. $J_{\rm r}/J_{\rm s}$ is weakly affected by N and the field direction. $J_{\rm r}/J_{\rm s}(N=\infty)$ decreases with the increase of grain size L. These are larger than the experimental values for the Nd-rich $Nd_{2.33}Fe_{14}B_{1.06}Si_{0.21}$ magnets by $\sim$0.05. ${}_{\rm i}H_{\rm c}(N=\infty)$ increases with the increase of L, and is close to or somewhat smaller than the experimental values of the Nd-rich magnet, as would be expected. In contrast, the curve calculated for the non-interacting grain system (Stoner–Wohlfarth model) of $N \geq 30$ depends neither on the field direction nor on N.

Keywords: rare-earth Fe compound, high coercive force materials, magnetization curves, hysteresis loop, micromagnetism
PACC: 7550B, 7560E, 7550K, 7560G

I. INTRODUCTION

Since 1996, many calculations have been reported on the demagnetization curves for nanocrystalline Nd–Fe–B magnets, using the finite element technique of micromagnetics, mostly by the group Fischer *et al.*[1] The quality of the calculations are not satisfactory. For example, the values of ${}_{\rm i}H_{\rm c}$, calculated as a function of the grain size L for the stoichiometric composition, are greater than the experimental values for the Nd-rich $Nd_{2.33}Fe_{14}B_{1.06}Si_{0.21}$ magnets[2] by as much as (60–170)%[1] in contrast to the fact that they should be smaller. Since the inter-grain exchange interaction for the magnet of stoichiometric composition with the $Nd_2Fe_{14}B$ grains in direct contact is stronger than that for Nd-rich magnets with the Nd-rich paramagnetic boundary phase separating the grains, ${}_{\rm i}H_{\rm c}$ of the former should be smaller than that of the latter. Griffiths *et al.*[3] simulated the ${}_{\rm i}H_{\rm c}$-L relation with a much better quality by including a grain number N larger than 35, its value in Ref.[1].

Recently, we found that the calculated demagnetization curve, especially ${}_{\rm i}H_{\rm c}$, strongly depends on the direction of the applied field if N is taken to be small.[4,5] Apparently the demagnetization curve calculated along an arbitrarily selected field direction for small N has only a qualitative meaning. This paper will present the details of the anisotropic characteristics and an approach to obtain a quantitative simulation of the demagnetization curves.

II. MODELS AND CALCULATIONS

The cubic magnet consists of $N = n \times n \times n$ cubic grains of size L. The c axes of the grains are distributed nearly uniformly in the 4π solid angle space and are assigned to the grains randomly to simulate the isotropy of the real magnets. Each grain is divided into $m_{\rm r} \times m_{\rm r} \times m_{\rm r}$ cubic regions of dimension $L/m_{\rm r}$. Two models, model G and model S, are considered. The Stoner–Wohlfarth (S–W) model is also considered for reference. In the S–W model, $m_{\rm r}$=1 and the grains are single domains without interactions between them. Model G is the same as that of Griffiths *et al.*[3] and each region is a uniformly magnetized single domain element exchange coupled with the six adjacent elements. Model S is somewhat similar to that of Fischer *et al.*[1] and each cubic region is subdivided further into 24 tetrahedral elements. The four

*Project supported by the National Natural Science Foundation of China (Grant No. 59871019).

vertices of the tetrahedron are the cubic centre, the centre of a surface, and two vertices of the surface of the cubic region (CC, FC, V1 and V2, respectively, in Fig.1). The magnetic polarization in the element is a linear function of the magnetic polarizations on the four vertices. In a brief summary, the grain is divided into $(m\times m\times m)$ elements, where $m = m_{\rm r}$ for model G and $m = m_{\rm r}\times 24^{1/3}$ for model S. The magnet is piled up periodically in the whole space and the periodic boundary conditions of the magnetic properties hold for a magnet.

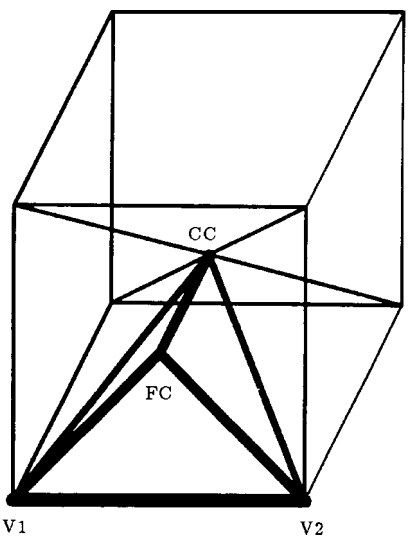


Fig.1. A tetrahedral element {CC, FC, V1, V2} in model S: CC, cubic centre; FC, centre of a face of the cube; V1 and V2, vertices of the cube.

By neglecting the stray field energy which plays a minor role for the Nd–Fe–B magnet of large magnetocrystalline anisotropy,[6] the Gibb's free energy of the magnet is

$$F = \int [A\sum_i (\nabla\alpha_i)^2 + K_1\sin^2\theta_{<100>} + K_2\sin^2\theta_{<100>} - \boldsymbol{J}_{\rm s}\cdot\boldsymbol{H}]{\rm d}v. \quad (1)$$

Here $\alpha_i (i{=}x, y, z)$ are the direction cosines of the magnetic polarization $\boldsymbol{J}_{\rm s}$ and $\theta_{\langle 100\rangle}$ is the angle between $\boldsymbol{J}_{\rm s}$ and the c axis. The values of the magnetic constants for $Nd_2Fe_{14}B$ are $J_{\rm s}$=1.63T, A=7.7×10^{-12}J/m, K_1=4.3×10^{6}J/m^3 and K_2=0.65×10^{6}J/m^3 at room temperature.[1] The K_2 term is neglected unless mentioned otherwise. The applied field is decreased from 5T by step $\Delta\mu_0 H$=0.1T and the polarization J at each field is obtained from a minimization of the energy with respect to the directions of the polarization of the elements (model G) or of the polarization at the vertices of the tetrahedral elements (model S).

The minimization of energy was obtained by using the conjugate gradient method.[7] The Gaussian–Seidel (G–S) method[8,9] with a step increment of $\{\Delta\theta_i, \Delta\varphi_i\} = 2^\circ$ was also used in some cases for model G for reference. Here (θ_i, φ_i) are the polar angles of $\boldsymbol{J}_{\rm s}$ of the ith element in the coordinate system fixed on the magnet. A smaller step increment for better accuracy is not workable for large m due to the CPU time being too large.

As is well established, the 180° domain wall energy γ and structure (the variation of the angle between $\boldsymbol{J}_{\rm s}$ and the c axis across the wall $\theta(z)$) are given by the relations

$$\gamma = \int_{-\infty}^{\infty} [A({\rm d}\theta/{\rm d}z)^2 + K_1\sin^2\theta]{\rm d}z = 4\sqrt{AK_1}, \quad (2)$$

$$\frac{z(\theta)}{\delta_0} = \ln\left(\tan\frac{\theta}{2}\right), \qquad \delta_0 = \sqrt{\frac{A}{K_1}}. \quad (3)$$

The domain wall width is $\delta = \pi\delta_0$=4.2nm. The energies for the one-dimensional model G, $\gamma_{\rm G}$, and that for model S, $\gamma_{\rm S}$, are calculated by replacing the integration by the sum of the discrete energies of the one-dimensional elements of dimension d as

$$\gamma_{\rm G} = d\sum_i \left[A\left(\frac{\theta_{i+1}-\theta_i}{d}\right)^2 + K_1\sin^2\theta_i\right], \quad (4)$$

$$\gamma_{\rm S} = d\sum_i A\left(\frac{\theta_{i+1}-\theta_i}{d}\right)^2 + \sum_i \int_0^d K_1\sin^2\left(\theta_i + \frac{\theta_{i+1}-\theta_i}{d}z\right){\rm d}z \quad (5)$$

(i : integer, $-1000\ \delta_0/d \le i \le 1000\ \delta_0/d$; $\theta_{-1000\ \delta_0/d} = 0$ and $\theta_{1000\ \delta_0/d} = 180^\circ$).

Ⅲ. RESULTS AND DISCUSSION

A. Demagnetization curve versus grain number and field direction for the S–W model

Figure 2 depicts the demagnetization curves calculated, using the S–W model for n=3, 5, 8 and ∞ (N=27, 125, 512 and ∞). There are four curves along four arbitrarily selected H directions ($0^\circ \le \theta_{\rm H} < 180^\circ, 0^\circ \le \varphi_{\rm H} < 360^\circ$), for each n, which are compared with that for $n = \infty$. It can be seen that the curve is essentially independent of $n(\ge 3)$ and is isotropic against the applied field direction.

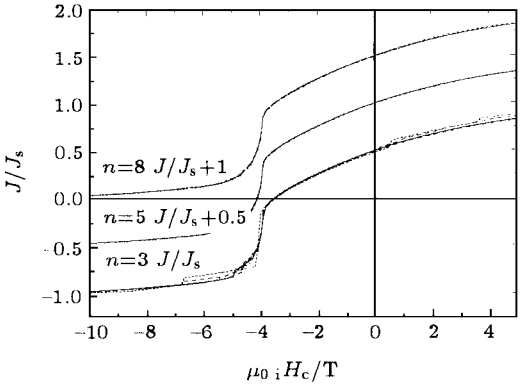


Fig.2. The demagnetization curves calculated using the S–W model for n=3, 5, 8 and ∞. Solid, dotted, dashed and short-dashed lines for each n calculated, respectively, along four arbitrarily selected field directions. The open circles represent $n = \infty$.

B. 180° domain wall energy and structure versus element dimension

The wall energies and the centre part of the 180° domain wall, which is a most inhomogeneous region of $\boldsymbol{J}_s$ distribution, were examined for models G and S. Figure 3(a) shows the reduced 180° domain wall energies γ_G/γ and γ_S/γ as functions of the reduced element dimension d/δ_0. The results demonstrates that the refinement of the elements to a dimension smaller than $1.5\delta_0$ ≈2nm≈ $\delta/2$ gives a fairly accurate energy with the error smaller than ±2%. The seemingly unreasonable result that γ_G is smaller than the theoretical lower limit of γ in the range of $0 < d/\delta_0 <\sim 1.8$ is not false. In fact, it is assumed in Eq.(4) that θ varies with z linearly between the centres of adjacent elements (denoting the variation by $\theta_1(z)$) for the calculation of the exchange energy $\gamma_{ex}(\theta_1(z))$, while it remains constant within each element and varies stepwise at the element boundary (denoting the variation by $\theta_2(z)$) for the calculation of the magnetocrystalline anisotropy energy $\gamma_K(\theta_2(z))$. Since $\theta_1(z) \neq \theta_2(z)$, $\gamma_G = \gamma_{ex}(\theta_1(z))+\gamma_K(\theta_2(z)) \approx \gamma$ is not bound to be larger than γ.

Figure 3(b) shows θ as a function of reduced distance from the centre of the wall z/δ_0 calculated by model G and model S for d/δ_0=1.3 (d=1.7nm) along with the theoretical relation of Eq.(3). It can be seen that both models with the element dimension of ∼40% of the domain wall width simulate the domain wall structure very well.

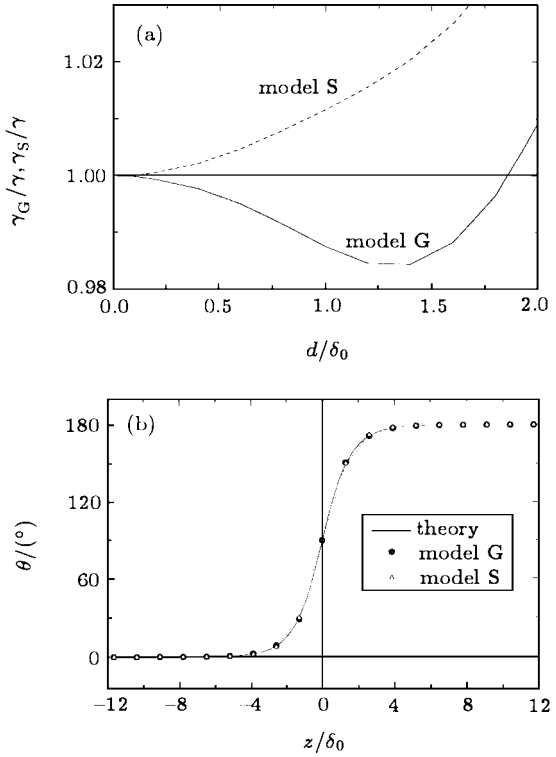


Fig.3. The reduced 180° domain wall energy as a function of the reduced dimension of the element for models G and S (a), and the domain wall structure of model G (solid circle), model S (open triangle + dotted line) and Eq.(3) (solid line) (b).

C. Demagnetization curve versus element dimension

Figure 4 shows the demagnetization curves calculated, using model S for L=10nm, n=3 and different m_r.

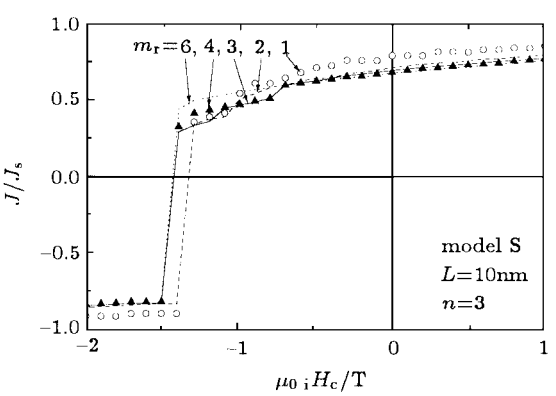


Fig.4. The demagnetization curves calculated, using model S: L=10nm; n=3; and m_r=1 (open circles), 2 (dashed curve), 3 (solid curve), 4 (solid triangles) and 6 (dotted curve).

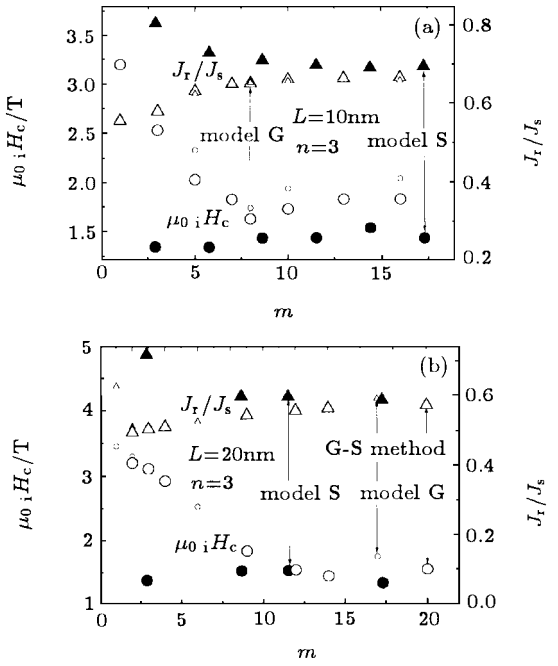


Fig.5. J_r/J_s (triangles) and $\mu_0\,{}_iH_c$ (circles) as a function of m for n=3: open symbols, model G; solid symbols, model S. (a) L=10nm; larger open symbols, K_2=0; smaller open symbols, K_2=0.65×10^{6}J/m^3. (b) L=20 nm; open larger symbols, the conjugate gradient method; smaller open symbols, the G–S method.

Figures 5(a) and 5(b) show J_r/J_s and $\mu_0\,{}_iH_c$ as functions of m for n=3 and L=10nm (Fig.5(a)) and 20nm (Fig.5(b)). For L=10nm (Fig.5(a)) J_r/J_s increases for model G and decreases for model S with the increase of m and approaches a common limit of $J_r/J_s \approx 0.68$ within ±0.03 when m increases above 7. The figure demonstrates that the inclusion of the K_2 term affects J_r/J_s only a little. With the increase of m, $\mu_0\,{}_iH_c$ decreases to a minimum around m=8 and then increases slightly for model G while it increases slowly for model S. $\mu_0\,{}_iH_c$ approach their common limit of 1.6T within ±0.2T when m is increased above 7, i.e. the dimension of the element L/m is decreased below 1.4nm≈ $\delta/3$. The figure demonstrates that the value of $\mu_0\,{}_iH_c$ is increased by 0.2±0.1T if the K_2 term is included. The variations of J_r/J_s and $\mu_0\,{}_iH_c$ with m for L=20nm (Fig.5(b)) are similar to that for L=10nm (Fig.5(a)), and the limits of J_r/J_s and $\mu_0\,{}_iH_c$ are 0.58±0.01 and 1.5±0.1T, respectively. The limits are almost reached when m is increased to ∼10, i.e. the dimension of the element is decreased to ∼2nm≈ $\delta/2$. Figure 5(b) also demonstrates that the results obtained by the G–S method are nearly the same or slightly larger than those obtained by the conjugate-gradient method. It is expected that the difference could be narrowed by decreasing the step of $\{\Delta\theta_i, \Delta\varphi_i\}$. Summarizing the above results, it is concluded that the division of the grain into elements of dimension around 1.5±0.5nm≈(1/4–1/2)δ is reasonable for the analysis of the demagnetization curves. A refinement of the dimension below the lattice constants (a=0.881nm, c=1.221nm) would be physically meaningless. In such a case the magnetic properties become different for different elements and it becomes inadequate to describe them by the macroscopic parameters of J_s, A and K_i (i=1,2) by assuming that the properties are the same for all elements.

D. Demagnetization curve versus grain number and field direction

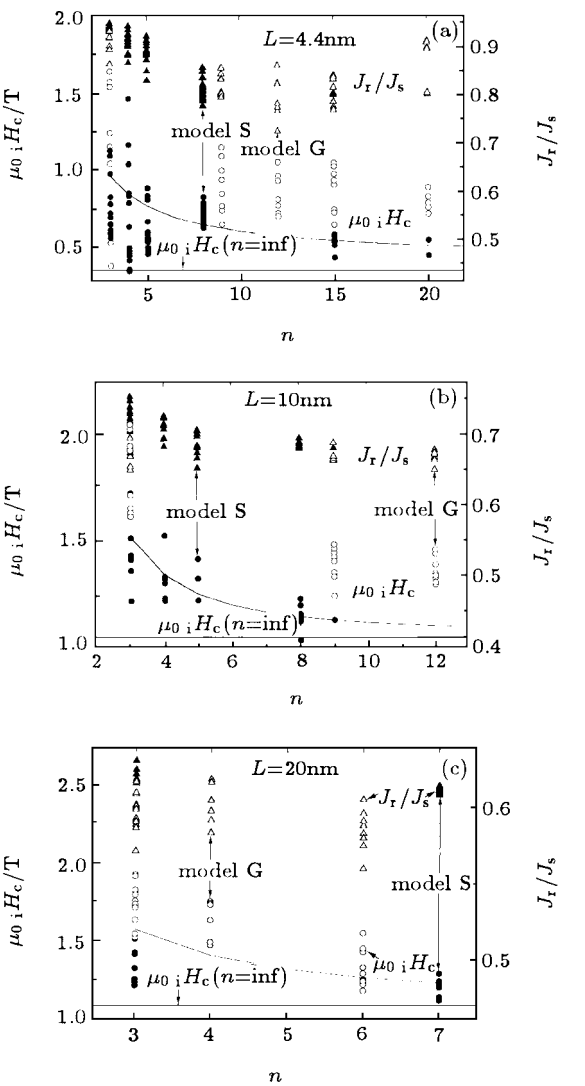


Fig.6. J_r/J_s (triangles) and $\mu_0\,{}_iH_c$ (circles) along different H directions as a function of n: open symbols, model G; solid symbols, model S; solid curves, Eq.(6) and Table 1; solid straight lines, $\mu_0\,{}_iH_c(n=\infty)$. (a) L=4.4nm; m=4 (L/m=1.1nm) for model G and m=2.88 (m_r=1, L/m=1.5nm) for model S. (b) L=10nm; m=7 (L/m=1.4nm) for model G and m=8.65 (m_r=3, L/m=1.2nm) for model S. (c),L=20nm; m=14 or 16 (L/m=1.3–1.4nm) for model G and m=11.54 (m_r=4, L/m=1.7nm).

The demagnetization curves for different grain numbers were calculated along several arbitrarily selected field directions. Figures 6(a)–6(c) show J_r/J_s and $\mu_0\ {}_iH_c$ as functions of n for the grain sizes L=4.4nm (Fig.6(a)), 10nm (Fig.6(b)) and 20nm (Fig.6(c)). The different values of J_r/J_s and $\mu_0\ {}_iH_c$ corresponding to a given n are for different H directions. The dimensions of the elements are 1.1–1.7nm (see the figure captions for details).

It is striking that the demagnetization curve is dependent not only on n but also on the field direction. The result is in sharp contrast to the result of the S–W model for which the curve is dependent neither on n nor on the field direction.

The variation of the demagnetization curve with the field direction (θ_H, φ_H) for a given number of grains is complicated, as is demonstrated for $\mu_0\ {}_iH_c$ in Fig.7. The range of the variation of $\mu_0\ {}_iH_c$ along different field directions is unexpectedly large for small n. The range and average value of $\mu_0\ {}_iH_c$ for given n are larger for model G than model S. For both models the range and average decrease with the increase of n, and the average value approaches a limit. For example, for L=4.4nm the range decreases from 0.4–1.7T to 0.6–1.0T for model G. In contrast, the range decreases from 0.6–1.2T to 0.4–0.6T for model S, when n increases from 3 to 15 (N from 27 to 3375). The ranges are for around ten field directions and should increase further if the calculations are carried out along more field directions.

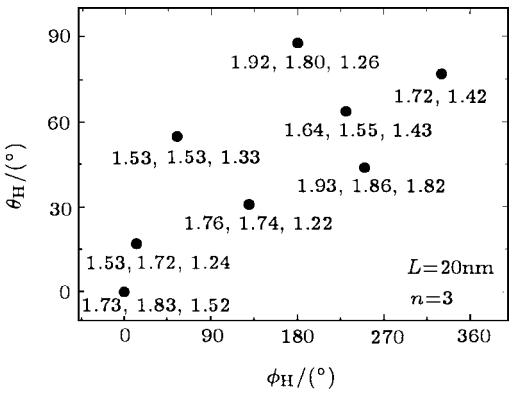


Fig.7. $\mu_0\ {}_iH_c$ versus field direction for L=20nm and n=3. The coordinates (θ_H, φ_H) of the solid circles are the field direction. The three numerals below the circles are the values of $\mu_0\ {}_iH_c$; from left to right, they are for the model G with m=14, model G with m=16 and model S with m=11.5 (m_r=4), respectively. The absence of the numeral in some spaces means that the value was not calculated.

The limit values of the coercive force $\mu_0\ {}_iH_c(n=\infty)$ were estimated by fitting the variation of $\mu_0\ {}_iH_c$ with n by the relation

$$\mu_0\ {}_iH_c(n) = \frac{C}{n^t} + \mu_0\ {}_iH_c(n=\infty), \qquad (6)$$

where C, t and $\mu_0\ {}_iH_c(n=\infty)$ are the fitting parameters which are listed in Table 1 for each L. The figures depict the above relation and the straight lines $\mu_0\ {}_iH_c(n=\infty)$-n.

Table 1. The values of C, t, $\mu_0\ {}_iH_c(n=\infty)$ and $J_r/J_s(n{=}\infty)$.

L/nm	C/T	t	$\mu_0\ {}_iH_c(n=\infty)$/T	$J_r/J_s(n=\infty)$
4.4	1.40	0.77	0.35	0.79
10	2.75	1.60	1.05	0.65
20	2.37	1.45	1.1	0.62
30	–	–	1.04	0.57

The value of $\mu_0\ {}_iH_c$ calculated so far for finite n along any field direction is larger than, or at least equal to, $\mu_0\ {}_iH_c(n=\infty)$. Hence the smallest value of $\mu_0\ {}_iH_c$ among those for different field directions and n is the closest one to the limit value $\mu_0\ {}_iH_c(n=\infty)$. This result was used to estimate the value of $\mu_0\ {}_iH_c(n=\infty)$ for the grain size L=30nm (Table 2).

The range of the variation of J_r/J_s is considerably small and decreases slightly with the increase of n, so that it decreases from 0.65–0.76 to 0.66–0.69 with the increase of n from 3 to 9 for L=10nm. The limit values of J_r/J_s are estimated directly from the figures and are also listed in Table 1.

Table 2. The values of $\mu_0\ {}_iH_c(\theta_H, \varphi_H)$ and $J_r/J_s(\theta_H, \varphi_H)$ for L=30nm, n=5, m_r=5 ($d \approx 0.5\delta$).

$\theta_H/(°)$, $\varphi_H/(°)$	$\mu_0\ {}_iH_c$/T	J_r/J_s
0, 0	1.24	0.569
17, 31	1.14	0.574
31, 130	1.23	0.574
44, 250	1.04≈ $\mu_0\ {}_iH_c(n=\infty)$	0.570
64, 131	1.24	0.569
88, 180	1.22	0.563

The anisotropic characteristics of the curve for finite N are expected from the discrete distribution of N c axes, distributed nearly uniformly in the 4π solid angle space. In the case of $N \approx 30$, for instance, a c axis makes an angle of around 30° with the neighbouring c axes in the solid angle space. The change of the field direction causes the change of the angles between the field direction and the c axes, which affects the demagnetization process, hence causing the change in the demagnetization curve. With the increase of N to infinity, the angle between the neighbouring c axes in the solid angle space decreases to zero, causing the decrease of the anisotropy to zero. The fact that the curves calculated by the S–W model are essentially isotropic ($n \geq 3$) shows that the inter-grain exchange interaction, which makes the demagnetization processes of the grains realized in a unified noncoherent rotation,[6,9] is also a key factor contributing to the anisotropic characteristics of the curve.

E. $J_r/J_s(n = \infty)$ and $\mu_0\ {}_iH_c(n = \infty)$ versus grain size L

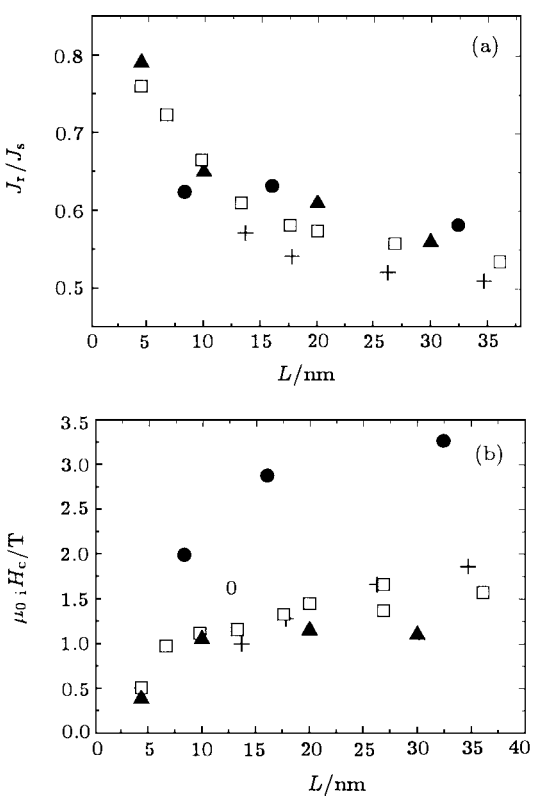


Fig.8. J_r/J_s (a) and $\mu_0\ {}_iH_c$ (b) as a function of L: solid triangles, this work; crosses, experiments[2]; solid circles, calculations[1]; open squares, calculations[3].

Figures 8(a) and 8(b) show the L dependence of $J_r/J_s(n=\infty)$ and $\mu_0\ {}_iH_c(n=\infty)$, respectively. The experimental results for $Nd_{2.33}Fe_{14}B_{1.06}Si_{0.21}$ [2] and the calculated results of Refs.[1,3] are also presented for reference.

With the increase of L, J_r/J_s decreases monotonically from 0.79 at L=4.4nm to 0.57 at L=30nm, which agree with the results of Refs.[1,3] fairly well and are larger than the experimental values by ~0.05. It is well established that the remanence increases with the increase of the inter-grain exchange interaction. Since the inter-grain exchange interaction in the calculations for the magnet without the grain boundary is larger than that in the experiment of the $Nd_{2.33}Fe_{14}B_{1.06}Si_{0.21}$ magnet with the Nd-rich paramagnetic boundary phase, the above result is reasonable.

Our results for $\mu_0\ {}_iH_c$ are close or somewhat smaller than the experimental values.[2] These results are expected because $\mu_0\ {}_iH_c$ decreases with the increase of the inter-grain exchange interaction, and $\mu_0\ {}_iH_c$ calculated for the magnet without the grain boundary phase should be smaller than that for the Nd-rich Nd–Fe–B magnets with smaller inter-grain exchange interaction.

In summary, the demagnetization curve, especially ${}_iH_c$, for the exchange coupled grain system of small N, calculated by using the finite element technique of micromagnetics, is strikingly anisotropic with respect to the field direction. With the increase of N, the range of the variation of ${}_iH_c$ with the field direction becomes smaller, and the values of ${}_iH_c$ decrease and approach a limit. The range and the average value of ${}_iH_c(N)$ for model S are smaller than those for model G. The smallest value of ${}_iH_c$ among those calculated along different field directions for a given N is larger than, or at most equal to, the limit value of ${}_iH_c(N = \infty)$. J_r/J_s is affected weakly by the field direction and N. For the isolated single domain grain system, the demagnetization curve is essentially independent of the field direction and N for $N \geq 27$.

According to the above results, we should obtain the limit curve corresponding to $N \to \infty$ for quantitative analyses. For this purpose a number of curves for several values of N and several field directions should be calculated in advance. By taking such an approach, the dependence of the demagnetization curve on the grain size (section E) and temperature[10] can be satisfactorily simulated quantitatively.

References

[1] Fischer R, Schrefl T, Kronmüller H and Fidler J 1996 *J. Magn. Magn. Mater.* **153** 35

[2] Manaf A, Buckley R A, Davies H A and Leonowicz M 1991 *J. Magn. Magn. Mater.* **101** 360

[3] Griffiths M K, Bishop J E L, Tucker J W and Davies H A 1998 *J. Magn. Magn. Mater.* **183** 49

[4] Jin H M, Zhao S F, Wang X F and Yan Y 1999 *Proc. 1st Int. Symp. on Magnetic Materials and Applications* (Korea: Taejon) p 67

[5] Jin H M, Zhao S F and Wang X F 2000 *J. Mater. Sci. Technol.* **16** 107

[6] Jin H M, Kim Y B and Wang X F 1998 *J. Phys.: Condens. Matter* **10** 7243

[7] Gill P, Murray W and Wright M H 1981 *Practical Optimization* (London: Academic)

[8] Torre E D 1986 *IEEE Trans. Magn.* **22** 484

[9] Jin H M, Kim Y B, Park W S, Park M J and Wang X F 1998 *J. Phys.: Condens. Matter* **10** 389

[10] Zhao S F, Jin H M, Wang X F and Yan Y 2001 *J. Phys.: Condens. Matter* to be published